Dynamic Stresses Induced within Rock in Case of Blasting with One Free Face

By

Ichiro ITO* and Koichi SASSA*

(Received August 28, 1963)

In this study, the behaviour of the dynamic principal stresses induced within rock by an explosion under confined condition was analyzed in case of blasting with one free face by applying the values of measured radial displacement, particle velocity and so on to equations derived from the theory of elasticity, and at the same time, the dynamic stresses on the free face were also calculated from the strain measured by the wire strain gauges affixed on the free face. The results obtained are briefly shown below.

1) The maximum stress on the free face appeared at the intersection between the free face and the burden, and its magnitude was about twice as large as the magnitude of the tangential tensile stress imparted by the incident stress wave within the range related to the breakage by blasting.

2) The maximum value of the compressive stress near the free face was decreased due to the existence of the free face, while that of the tensile stress was increased.

3) Let us consider the spherical coordinate of which origin is the center of a spherical charge. Then, at any point near the free face, the directions of the principal stresses in the $r\theta$ plane changed with time except in the direction of the burden, but at another point near an explosion point where the principal stresses were mainly composed of the stresses caused by the initial longitudinal wave, the directions of the principal stresses coincided with those of the coordinate used.

4) The maximum value of the tensile stress in ϕ direction was larger than those in the $r\theta$ plane on and near the free face.

5) The tensile stress caused by the Hopkinson effect appeared only near the burden.

6) It is presumed from the results of stress analysis that radial cracks will be produced in the rock mass near an explosion point, but with the approach of the free face the directions of the cracks will be curved towards the direction parallel to the free face.

7) The appearance of the breakage deduced from this investigation agrees fairly well with the practical observations.

1. Introduction

In order to investigate the mechanism of rock breakage by blasting, it is considered to be very important to know how the stresses are generated and

* Department of Mining Engineering

distributed within rock by an explosion of a confined charge. Then, as a part of researches concerning the mechanism of rock breakage by blasting, the authors have already published papers on the detonation pressure produced at the inner surface of the charge hole[1] and on the behaviour of the dynamic stresses within rock caused by an explosion in the case where no free face existed[2].

Therefore, in this study the dynamic stresses on and near the free face have been investigated in case of blasting with one free face, and by using the results of these studies the mechanism of rock breakage by blasting has been discussed.

2. Stress Wave Projected into Rock Mass by the Detonation of a Detonator

2.1. Method of stress analysis

The relations which are used to calculate the dynamic stresses in the stress wave are shown simply below because of the process for deriving these relations from the theory of elasticity has been discussed in detail in the previous paper[3]. Now, let us consider a spherical coordinate (r, θ, ϕ) of which origin is at the center of a spherical charge within a homogeneous, ideally elastic, infinite medium of density ρ. The radial stress $\widehat{rr}$ and the tangential stresses $\widehat{\theta\theta}$, $\widehat{\phi\phi}$ in the stress wave can be shown by the following expressions.

$$\left.\begin{aligned} \widehat{rr} &= (\lambda+2\mu)\left\{\frac{du_p(r)}{dr}\cdot u_W(\tau)-\frac{v(r,\tau)}{C_L}\right\}+2\cdot\lambda\frac{u(r,\tau)}{r}, \\ \widehat{\theta\theta} &= \widehat{\phi\phi} = \lambda\left\{\frac{du_p(r)}{dr}\cdot u_W(\tau)-\frac{v(r,\tau)}{C_L}\right\}+2(\lambda+\mu)\frac{u(r,\tau)}{r}, \\ \widehat{r\theta} &= \widehat{\theta\phi} = \widehat{\phi r} = 0, \end{aligned}\right\} \quad \cdots\cdots(1)$$

where, $u(r,\tau) = u_p(r)\cdot u_W(\tau)$, $\cdots\cdots(2)$

$\tau = t - r/C_L$, $\cdots\cdots(3)$

and $u(r,\tau)$: Radial elastic displacement,

$v(r,\tau)$: Radial particle velocity,

$u_p(r)$: Function of r which determines the maximum value of the displacement,

$u_W(\tau)$: Function of τ which indicates the change in the magnitude of radial elastic displacement with time,

t : Time from the instant of detonation,

C_L : Propagation velocity of longitudinal wave in the rock,

λ, μ : Lamé's constants.

Therefore, the stresses at any point in the medium can be analyzed by measuring $u(r,\tau)$; $v(r,\tau)$; the derivative of the maximum displacement with distance,

$du_p(r)/dr$; ρ; C_L and C_T, where C_T denotes the propagation velocity of a transverse wave in the rock.

2. 2. Displacement and particle velocity caused by the detonation of a detonator

In this study, a kind of sandstone which was formed in a rectangular hexahedron of 60 cm × 60 cm × 40 cm was used as the rock mass, and the displacement and the particle velocity which were induced within it by the detonation of a detonator of No. 1 strength under confined condition were measured by using an accelerometer. Experimental procedure and arrangement of recording apparatuses were similar to those written in the previous paper. The values of the displacement and the particle velocity which were measured on the free face were corrected into those which could be expected in the case where no free face existed.

The relations of the maximum values of the displacement and the particle velocity with distance obtained in this experiment are shown in Fig. 1. The decay of these values with distance can be indicated approximately by the following expressions,

$$u_p(r) = A_0 \cdot r^{-2.2} \quad (10\,\text{cm} < r < 20\,\text{cm}), \cdots (4)$$

$$u_p(r) = A' \cdot r^{-2.0} \quad (20\,\text{cm} < r < 40\,\text{cm}), \cdots (5)$$

$$v_p(r) = B_0 \cdot r^{-2.0}, \cdots (6)$$

where A_0, A' and B_0 are the constants. Moreover, Fig. 2 shows the changes in the displacement and particle velocity with time obtained at the point of $r = 12$ cm.

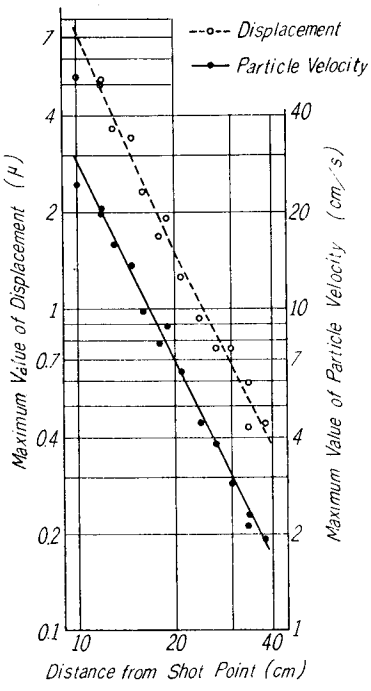

Fig. 1. Logarithmic plots of the maximum values of displacement and particle velocity against distance.

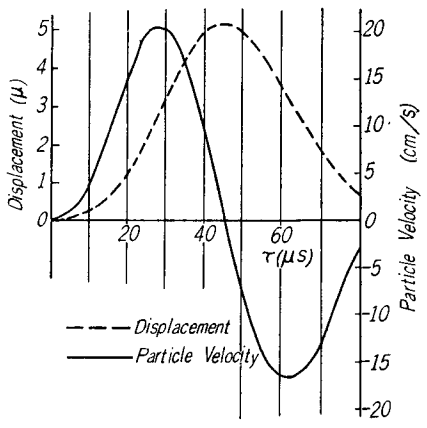

Fig. 2. Changes in displacement and particle velocity with time

2.3. Magnitudes of stresses in the stress wave

At the first time, the values, $\lambda=2.69\times10^7$ g/cm², $\mu=5.55\times10^7$ g/cm², $C_L=2{,}600$ m/s, $C_T=1{,}700$ m/s and $\rho=2.0$ g/cm³ were determined for the rock mass used. The magnitudes of the stresses in the stress wave were analyzed by applying the values of the displacement, the particle velocity and the above constants to equation (1). Logarithmic plots of the maximum values of the radial stress $\widehat{rr}$ and the tangential stress $\widehat{\theta\theta}$ $(=\widehat{\phi\phi})$ are shown in Fig. 3.

As the magnitudes of the stresses in such stress wave have been clarified by this study shown above, then, let us consider about the dynamic stresses induced on the free face by the reflection of the stress wave.

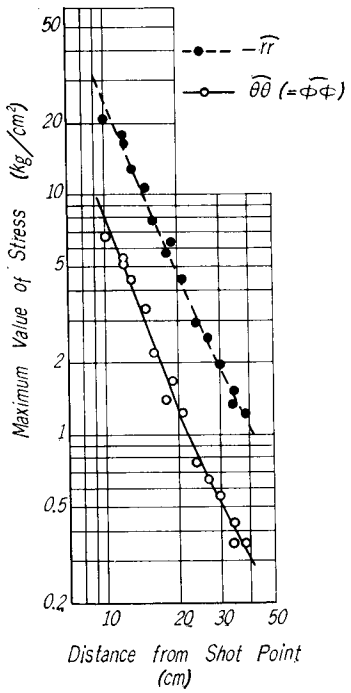

Fig. 3. Logarithmic plots of the maximum values of $\widehat{rr}$ and $\widehat{\theta\theta}$ against distance.

3. Dynamic Stresses Induced on the Free Face

3.1. Measurement of the dynamic stresses on the free face by using wire strain gauges

Now, let us consider a cylindrical coordinate (η, ψ, Z) as shown in Fig. 4. The stresses on the free face can be indicated by the following expressions,

$$\left.\begin{aligned}\widehat{\eta\eta} &= \frac{2}{\lambda+2\mu}\{2\mu(\lambda+\mu)e_{\eta\eta}+\lambda\cdot\mu\cdot e_{\psi\psi}\}\ ,\\ \widehat{\psi\psi} &= \frac{2}{\lambda+2\mu}\{2\mu(\lambda+\mu)e_{\psi\psi}+\lambda\cdot\mu\cdot e_{\eta\eta}\}\ ,\\ \widehat{ZZ} &= 0\ .\end{aligned}\right\} \quad \cdots(7)$$

In this experiment, the dynamic strains on the free face which were induced by the detonation of a detonator of No. 1 strength under the condition same as that in the above experiment were measured by using some wire strain gauges affixed at the points of $\eta=Z=0$ and $\eta=W$, $Z=0$, where W denotes the length of the burden.

The maximum values of $\widehat{\eta\eta}$ and $\widehat{\psi\psi}$ at the point of $\eta=Z=0$, which were obtained

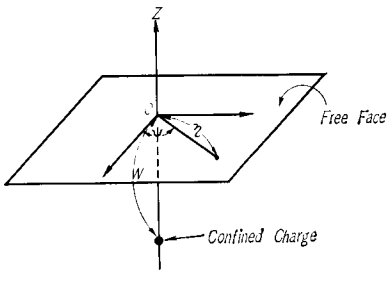

Fig. 4. Cylindrical coordinate adopted for analyzing the stresses on the free face.

Table 1. The maximum values of $\widehat{\eta\eta}$ and $\widehat{\psi\psi}$ at the point of $\eta=Z=0$, which were obtained by using wire strain gauges.

Hole number	Distance from shot point (cm)	Maximum value of $e_{\eta\eta}(=e_{\psi\psi})$	$\widehat{\eta\eta}_M(=\widehat{\psi\psi}_M)$ (kg/cm²)	$\dfrac{\widehat{\eta\eta}_M(=\widehat{\psi\psi}_M)}{\widehat{rr}}$	$\dfrac{\widehat{\eta\eta}_M(=\widehat{\psi\psi}_M)}{\widehat{\theta\theta}(=\widehat{\phi\phi})}$
S_5	17	1.83×10^{-5}	2.83	−0.46	1.4
S_6	17	1.80 "	2.33	−0.39	1.2
S_7	17	2.18 "	3.10	−0.47	1.6
S_8	17	1.22 "	1.88	−0.26	0.9
S_3	14	3.64 "	5.61	−0.50	1.7
S_5	14	2.65 "	4.10	−0.36	1.2
S_6	14	1.99 "	3.08	−0.27	0.9
S_7	14	3.58 "	5.52	−0.49	1.7
S_8	14	2.70 "	4.16	−0.37	1.3
S_5	11	5.45 "	8.42	−0.42	1.3
S_7	11	5.72 "	8.85	−0.44	1.4
S_8	11	4.85 "	7.50	−0.38	1.2
S_3	8	10.45 "	16.1	—	—
S_5	5	41.6 "	64.3	—	—
S_7	5	35.8 "	55.3	—	—

by substituting the measured values of the strain to equation (7), are summarized in Table 1. Besides those values $[\widehat{\eta\eta}_M(=\widehat{\psi\psi}_M)]$, the ratios of $\widehat{\eta\eta}_M(=\widehat{\psi\psi}_M)$ to the maximum radial and tangential stresses imparted by the incident stress wave are also shown in Table 1. As the examples of the strain oscillograms, those of the radial strain $e_{\eta\eta}$ obtained at the points of $\eta=Z=0$ and $\eta=10.5$ cm, $Z=0$ in case of $W=11$ cm are shown in Figs. 5 and 6. The maximum strain in the trace shown in Fig. 5 is a tensile one and its value is about 5.45×10^{-5}, but that shown in Fig. 6 is a compressive one and its value is about -3.2×10^{-5}. Therefore, it is under-

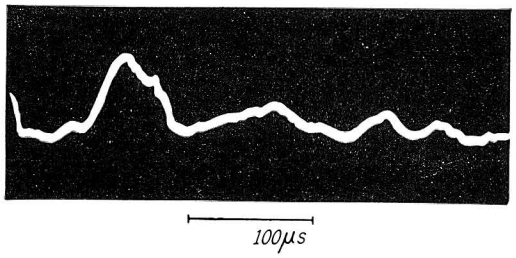

Fig. 5. An example of radial strain oscillograms (at the point of $\eta=Z=0$)

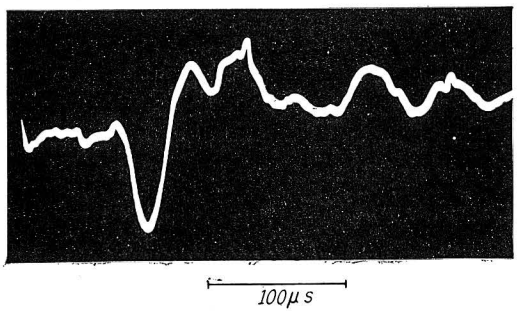

Fig. 6. An example of radial strain oscillograms (at the point of $\eta=10.5$ cm, $Z=0$)

stood that the maximum strain at the point of $\eta=W$, $Z=0$ has a character of a compressive one and its absolute value is about a half of that at the point of $\eta=Z=0$.

3.2. Consideration of these stresses by using the theory of reflection of elastic waves

Let us consider a cylindrical coordinate as shown in Fig. 4. The main wave projected into the surrounding rocks by an explosion of a confined spherical charge is a longitudinal wave, therefore, the components (u_η, u_ψ, u_Z) of the elastic displacement on the free face in η, ψ, Z directions can be shown by

$$u_\eta = w_\eta(\eta, \xi), \quad u_\psi = 0, \quad u_Z = w_Z(\eta, \xi). \qquad \cdots\cdots(8)$$

In case of the dynamic displacement, $w_\eta(\eta, \xi)$ can be indicated by the following form;

$$w_\eta(\eta, \xi) = w_{\eta p}(\eta) \cdot w_{\eta W}(\xi), \qquad \cdots\cdots(9)$$

$$\xi = t - [\sqrt{\eta^2 + W^2}/C_L], \qquad \cdots\cdots(10)$$

where, $w_{\eta p}(\eta)$: Function of η which determines the maximum value of $w_\eta(\eta, \xi)$,

$w_{\eta W}(\xi)$: Function of ξ which indicates the change in the magnitude of $w_\eta(\eta, \xi)$ with time.

Therefore by using the method similar to that used in the derivation of equation (1), the stresses on the free face are given by

$$\left.\begin{aligned}
\widehat{\eta\eta} &= \frac{2}{\lambda+2\mu}\left[2\mu(\lambda+\mu)\left\{\frac{dw_{\eta p}(\eta)}{d\eta}\cdot w_{\eta W}(\xi) - \frac{\sin i}{C_L}\cdot v_\eta(\eta, \xi)\right\} + \lambda\cdot\mu\frac{w_\eta(\eta, \xi)}{\eta}\right], \\
\widehat{\psi\psi} &= \frac{2}{\lambda+2\mu}\left[\lambda\cdot\mu\left\{\frac{dw_{\eta p}(\eta)}{d\eta} w_{\eta W}(\xi) - \frac{\sin i}{C_L}\cdot v_\eta(\eta, \xi)\right\} + 2\mu(\lambda+\mu)\frac{w_\eta(\eta, \xi)}{\eta}\right], \\
\widehat{ZZ} &= 0.
\end{aligned}\right\} \cdots(11)$$

Where, v_η: Component of particle velocity on the free face in η direction,

i : Incident angle of the longitudinal wave.

Now, the relation between the amplitude of the incident longitudinal wave at the free face and that of the vibration of rock particle at the free face can be obtained by using the theory of reflection of elastic waves. Therefore, the values of $w_\eta(\eta, \xi)$, $v_\eta(\eta, \xi)$ and $dw_{\eta p}(\eta)/d\eta$ can be calculated generally from the measured values of the displacement and the particle velocity shown in Paragraph 2.2. by applying this relation. But in this study this relation was calculated by assuming that the incident longitudinal wave projected by an explosion was a plane, elastic wave instead of a spherical one, therefore, the results shown below may include some errors based on the fact that a spherical wave is regarded as a plane one.

Table 2. The maximum values of $\widehat{\eta\eta}$ and $\widehat{\psi\psi}$ at the point of $\eta=Z=0$, which were obtained by using the theory of reflection of elastic waves.

Hole number	Distance from shot point (cm)	Maximum value of $e_{\eta\eta}(=e_{\psi\psi})$	$\widehat{\eta\eta}_G(=\widehat{\psi\psi}_G)$ (kg/cm²)	$\dfrac{\widehat{\eta\eta}_G(=\widehat{\psi\psi}_G)}{\widehat{rr}}$	$\dfrac{\widehat{\eta\eta}_G(=\widehat{\psi\psi}_G)}{\widehat{\theta\theta}(=\widehat{\phi\phi})}$
S_1	38.2	0.28×10^{-5}	0.45	−0.37	1.3
S_1	34.0	0.32 »	0.50	−0.37	1.4
S_2	34.0	0.44 »	0.68	−0.44	1.6
S_2	30.0	0.65 »	1.00	−0.51	1.8
S_1	27.0	0.71 »	1.10	−0.43	1.7
S_1	24.0	1.00 »	1.54	−0.53	2.0
S_2	21.0	1.51 »	2.33	−0.52	1.9
S_4	19.0	2.67 »	4.12	−0.65	2.4
S_2	18.0	2.38 »	3.68	−0.65	2.6
S_4	16.0	3.68 »	5.68	−0.74	2.4
S_1	14.8	5.85 »	9.02	−0.84	2.7
S_4	13.0	7.12 »	10.97	−0.85	2.5
S_1	12.0	11.0 »	16.93	−0.95	3.2
S_2	12.0	10.6 »	16.31	−0.97	3.2
S_4	10.0	13.4 »	20.70	−0.96	3.1

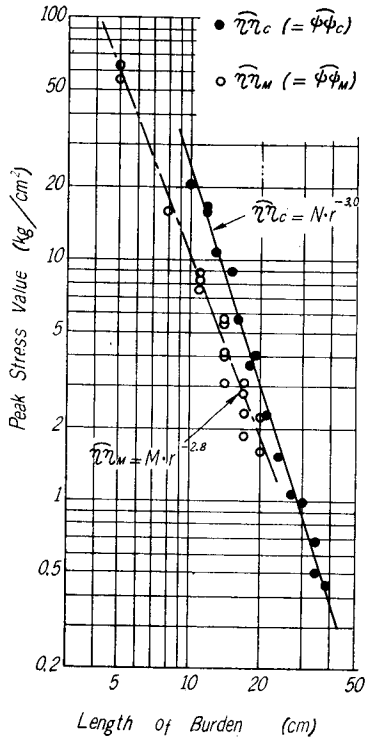

Fig. 7. Logarithmic plots of $\widehat{\eta\eta}_G$ and $\widehat{\eta\eta}_M$ against the length of the burden.

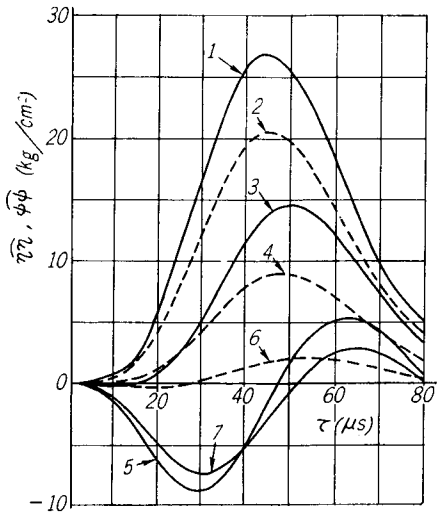

Fig. 8. Changes in $\widehat{\eta\eta}$ and $\widehat{\psi\psi}$ with time for the case of $W=10$ cm.

1 : Change in $\widehat{\eta\eta}(=\widehat{\psi\psi})$ at the point of $i=0°$
2 : Change in $\widehat{\psi\psi}$ at the point of $i=20°$
3 : Change in $\widehat{\eta\eta}$ at the point of $i=20°$
4 : Change in $\widehat{\psi\psi}$ at the point of $i=40°$
5 : Change in $\widehat{\eta\eta}$ at the point of $i=40°$
6 : Change in $\widehat{\psi\psi}$ at the point of $i=60°$
7 : Change in $\widehat{\eta\eta}$ at the point of $i=60°$

Both the maximum values of $\widehat{\eta\eta}$ and $\widehat{\phi\phi}$ at the point of $\eta=Z=0$ thus obtained and the ratios of these values to the maximum radial and tangential stresses imparted by the incident stress wave are shown in Table 2 and logarithmic plots of $\widehat{\eta\eta}_M(=\widehat{\phi\phi}_M)$ and $\widehat{\eta\eta}_C(=\widehat{\phi\phi}_C)$ against the length of the burden are shown in Fig. 7, where $\widehat{\eta\eta}_M(=\widehat{\phi\phi}_M)$ and $\widehat{\eta\eta}_C(=\widehat{\phi\phi}_C)$ are the maximum values of $\widehat{\eta\eta}$ and $\widehat{\phi\phi}$ on the free face which are obtained by the methods explained in Paragraphs 3. 1. and 3. 2. respectively. The changes in $\widehat{\eta\eta}$ and $\widehat{\phi\phi}$ with time at the points where the angle of incidence of the longitudinal wave was $0°(\eta=0)$, $20°(\eta=3.6\,\text{cm})$, $40°(\eta=8.4\,\text{cm})$ and $60°(\eta=17.3\,\text{cm})$ respectively were calculated for the case of $W=10\,\text{cm}$ and these results are shown in Fig. 8. Moreover, the relations of the maximum values of $\widehat{\eta\eta}$ and $\widehat{\phi\phi}$ to the reduced distance η/W are shown in Fig. 9.

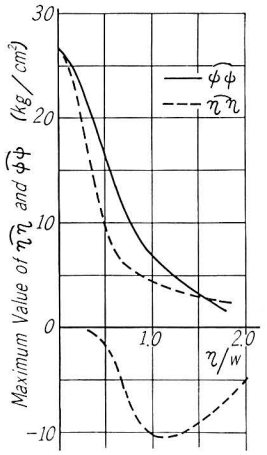

Fig. 9. Relations between η/W and the maximum values of $\widehat{\eta\eta}$ and $\widehat{\psi\psi}$.

3. 3. Summarized consideration on $\widehat{\eta\eta}$ and $\widehat{\phi\phi}$

As shown in Tables 1 and 2 and in Fig. 9, it is recognized that the maximum stress on the free face appears at the intersection of the burden to the free face, and its magnitude is about twice as large as the magnitude of the tangential stress imparted by the incident stress wave, and moreover the magnitude of the tangential tensile stress on the free face is always larger than that of the radial tensile stress within the range related to the breakage by blasting. Both of the stresses $\widehat{\eta\eta}$ and $\widehat{\phi\phi}$ at the point of $\eta=Z=0$ act as a nonoscillatory tensile stress and the change in those stresses with time are almost similar to that of the displacement, but the change in $\widehat{\eta\eta}$ with time

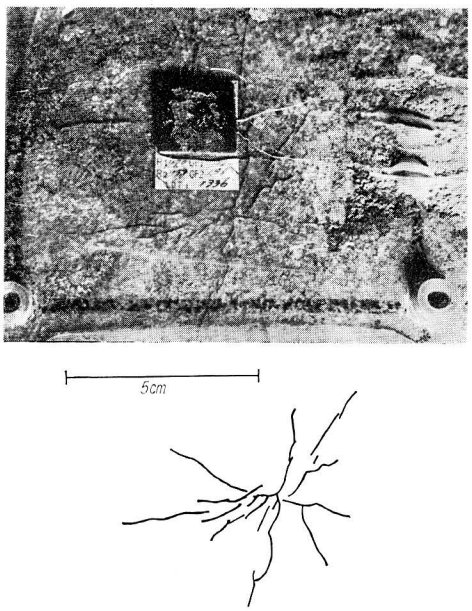

Fig. 10. Appearance of cracks on the free face.

becomes oscillatory with the increase of η as shown in Fig. 8. These facts can also be recognized by referring to Figs. 2, 5 and 6.

To make sure whether the results shown above were reasonable or not, some small scale blasting tests were carried out within the same rock mass. The cracks appeared on the free face after blasting are sketched and shown in Fig. 10. As shown in Fig. 10, it was found that the appearance of cracks on the free face agreed well with the one which can be expected from the result of these studies.

4. Dynamic Stresses Near the Free Face in Case of Blasting with One Free Face

4.1. Method of stress analysis

In case of blasting with one free face, the stresses at any point near the free face are induced by the superposition of the following three stresses as shown in Fig. 11; the first of them is the one produced by the longitudinal wave projected directly in rock by an explosion, and the second and the third ones are those produced by the reflected longitudinal and transverse waves which are projected from the free face by the reflection of the incident longitudinal wave. Hereafter these three waves are denoted as IP, RP and RS, and every quantity concerning these waves is indicated by the suffix *ip*, *rp* and *rs* respectively in this paper.

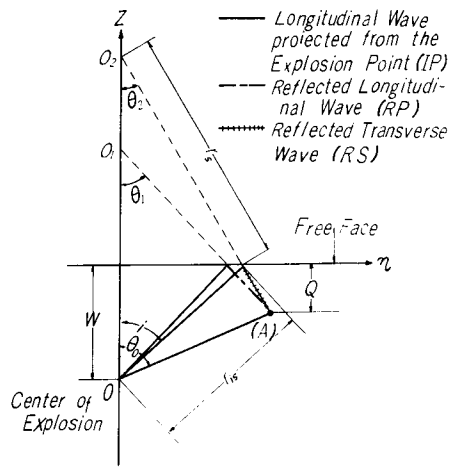

Fig. 11. Spherical coordinate adopted for analyzing the stresses near the free face.

In the first place, let us consider about the stresses caused by IP. As shown in Paragraph 2.1., these stresses can be calculated by equation (1). And furthermore, by referring to relations (4), (5) and (6), the displacement and the particle velocity produced by IP can be indicated generally by

$$\left.\begin{aligned} u(r, \tau_{ip}) &= A_0 \cdot r^{-n} u_W(\tau_{ip}), \\ v(r, \tau_{ip}) &= B_0 \cdot r^{-m} \cdot v_W(\tau_{ip}). \end{aligned}\right\} \quad \cdots\cdots(12)$$

Next, the analysis of the stresses caused by RP becomes more simple by using a spherical coordinate (r_1, θ_1, ϕ_1) of which origin (O_1) is a symmetric point of the charge (O) to the free face as shown in Fig. 11. By using this coordinate,

the displacement and the particle velocity caused by RP remain only in r_1 direction and those are given by

$$\left.\begin{aligned} u_1(r_1, \theta_1, \tau_{rp}) &= u_{p1}(r_1, \theta_1)\cdot u_{W1}(\tau_{rp}) = (A_r/A_e)A_0\cdot r^{-n}\cdot u_{W1}(\tau_{rp}), \\ v_1(r_1, \theta_1, \tau_{rp}) &= v_{p1}(r_1, \theta_1)\cdot v_{W1}(\tau_{rp}) = (A_r/A_e)B_0\cdot r^{-m}\cdot v_{W1}(\tau_{rp}). \end{aligned}\right\} \quad \cdots\cdots(13)$$

Where A_r/A_e which is a function of θ_1 indicates the ratio of the amplitude of RP to that of the incident longitudinal wave at the free face. Therefore, the stresses caused by RP are given by

$$\left.\begin{aligned} \widehat{rr}_{rp} &= (\lambda+2\mu)\left\{\frac{\partial u_{p1}(r_1, \theta_1)}{\partial r_1}\cdot u_{W1}(\tau_{rp}) - \frac{v_1(r_1, \theta_1, \tau_{rp})}{C_L}\right\} + 2\lambda\frac{u_1(r_1, \theta_1, \tau_{rp})}{r_1}, \\ \widehat{\theta\theta}_{rp} &= \widehat{\phi\phi}_{rp} = \lambda\left\{\frac{\partial u_{p1}(r_1, \theta_1)}{\partial r_1}\cdot u_{W1}(\tau_{rp}) - \frac{v_1(r_1, \theta_1, \tau_{rp})}{C_L}\right\} + 2(\lambda+\mu)\frac{u_1(r_1, \theta_1, \tau_{rp})}{r_1}, \\ \widehat{r\theta}_{rp} &= \mu\cdot\frac{1}{r_1}\cdot\frac{\partial u_{p1}(r_1, \theta_1)}{\partial\theta_1}\cdot u_{W1}(\tau_{rp}), \\ \widehat{\theta\phi}_{rp} &= \widehat{\phi r}_{rp} = 0, \end{aligned}\right\} \quad (14)$$

where, $\tau_{rp} = t - r_1/C_L$. $\cdots\cdots(15)$

Lastly, let us consider about the stresses due to RS. In this analysis, a spherical coordinate (r_2, θ_2, ϕ_2) of which origin is O_2 is adopted for simplifying the problem. By using this coordinate, the displacement and the particle velocity caused by RS remain only in θ_2 direction and those are given by

$$\left.\begin{aligned} u_\theta(r_2, \theta_2, \tau_{rs}) &= u_{\theta p}(r_2, \theta_2)\cdot u_{\theta W}(\tau_{rs}) = \frac{A_0}{r_{is}^n}\cdot\left(\frac{r_s}{r_2}\right)^l\cdot\frac{\mathfrak{A}_r}{A_e}\cdot u_{\theta W}(\tau_{rs}), \\ v_\theta(r_2, \theta_2, \tau_{rs}) &= v_{\theta p}(r_2, \theta_2)\cdot v_{\theta W}(\tau_{rs}) = \frac{B_0}{r_{is}^m}\cdot\left(\frac{r_s}{r_2}\right)^{l'}\cdot\frac{\mathfrak{A}_r}{A_e}\cdot v_{\theta W}(\tau_{rs}). \end{aligned}\right\} \quad \cdots\cdots(16)$$

Where $\mathfrak{A}_r/A_e$ is a function of θ_2 and it indicates the ratio of the amplitude of RS to that of the incident longitudinal wave, and l and l' are the decay exponents of the tangential displacement and particle velocity caused by RS. Therefore, the stresses induced by RS are given by

$$\left.\begin{aligned} \widehat{rr}_{rs} &= \lambda\left\{\frac{1}{r_2}\cdot\frac{\partial u_{\theta p}(r_2, \theta_2)}{\partial\theta_2}\cdot u_{\theta W}(\tau_{rs}) + \frac{u_{\theta p}(r_2, \theta_2)}{r_2}u_{\theta W}(\tau_{rs})\cdot\cot\theta_2, \right. \\ \widehat{\theta\theta}_{rs} &= (\lambda+2\mu)\cdot\frac{1}{r_2}\cdot\frac{\partial u_{\theta p}(r_2, \theta_2)}{\partial\theta_2}\cdot u_{\theta W}(\tau_{rs}) + \lambda\frac{u_{\theta p}(r_2, \theta_2)}{r_2}\cdot u_{\theta W}(\tau_{rs})\cdot\cot\theta_2, \\ \widehat{\phi\phi}_{rs} &= (\lambda+2\mu)\cdot\frac{u_{\theta p}(r_2, \theta_2)}{r_2}\cdot u_{\theta W}(\tau_{rs})\cdot\cot\theta_2 + \lambda\cdot\frac{1}{r_2}\cdot\frac{\partial u_{\theta p}(r_2, \theta_2)}{\partial\theta_2}\cdot u_{\theta W}(\tau_{rs}), \\ \widehat{r\theta}_{rs} &= \mu\left\{\frac{\partial u_{\theta p}(r_2, \theta_2)}{\partial r_2}\cdot u_{\theta W}(\tau_{rs}) - \frac{v_{\theta p}(r_2, \theta_2)}{C_T}\cdot v_{\theta W}(\tau_{rs}) - \frac{u_{\theta p}(r_2, \theta_2)}{r_2}\cdot u_{\theta W}(\tau_{rs}), \right. \\ \widehat{\theta\phi}_{rs} &= \widehat{\phi r}_{rs} = 0, \end{aligned}\right\} \quad (17)$$

where, $\tau_{rs} = t - \frac{r_{is}}{C_L} - \frac{(r_2 - r_s)}{C_T}$. $\cdots\cdots(18)$

The values of A_r/A_e and $\mathfrak{A}_r/A_e$ can be obtained by using the theory of reflection of elastic waves.

As shown above, the stresses caused by the respective stress waves can be calculated by using the respective equations in regard to the respective favourable coordinates. Accordingly, the stresses at any point within rock in case of blasting with one free face can be obtained by transferring these stress values to those for a common coordinate and synthesizing them.

4.2. Values of the constants for stress calculation

The values of λ, μ, C_L, C_T and ρ were already shown in Paragraph 2.3. In this study, the stresses were analyzed for the case of $W=10$ cm, therefore the values of every related factor were determined from the results of the experiments which were performed for the case of $W\cong 10$ cm. Both the values of A_0 and B_0 which determine the maximum values of the displacement and the particle velocity and the values of the decay exponents m and n can be determined from Fig. 1. Thus, the values of 0.123, 2.94×10^3, 2.0 and 2.2 were obtained as the values of A_0, B_0, m and n. To obtain the values of the decay exponents l and l', special experiments were performed within the same rock as the one used in the previous experiment and the identical value of 1.2 was obtained for both l and l'.

$u_{W1}(\tau_{rp})$, $u_{\theta W}(\tau_{rs})$ and $v_{W1}(\tau_{rp})$, $v_{\theta W}(\tau_{rs})$ were obtained from Fig. 2 assuming $u_{W1}(\tau_{rp})=u_{\theta W}(\tau_{rs})=u_W(\tau_{ip})_{\text{at } r=12\text{cm}}$ and $v_{W1}(\tau_{rp})=v_{\theta W}(\tau_{rs})=v_W(\tau_{ip})_{\text{at } r=12\text{cm}}$.

4.3. Method of stress calculation

It is clear from equations shown in Paragraph 4.1. that it needs much time to calculate the magnitude and the direction of the principal stresses induced within rock as the function of time. Therefore, those were calculated by using an electronic computer (KDC-1) taking intervals of 5μs from the instant of $\tau_{ip}=0$. By using this electronic computer, the time for calculating these stress values is only about 2 minutes per one point.

4.4. Behaviour of principal stresses near the free face

In this study, the behaviour of the principal stresses induced within a kind of sandstone by the detonation of a detonator of No. 1 strength under confined condition was studied for the case where the length of burden was 10 cm.

Now, let us consider a spherical coordinate (r, θ, ϕ) which is prescribed as the direction of Z axis coincides with that of the burden and the origin of this coordinate is a center of the charge, then one among three principal stresses within rock always acts in ϕ direction, but the directions of the other two principal stresses near the free face in the $r\theta$ plane change with time except

in the direction of the burden. Hereafter, the principal stress of which direction coincides with ϕ direction will be denoted as σ_3 and the other two in the $r\theta$ plane will be denoted as σ_1 and σ_2.

The behaviour of the principal stresses in the direction of the burden are shown in Fig. 12 [(a), (b), (c) and (d)]. In the direction of the burden, the principal stresses act always in r, θ, ϕ directions. Therefore in these figures, σ_1

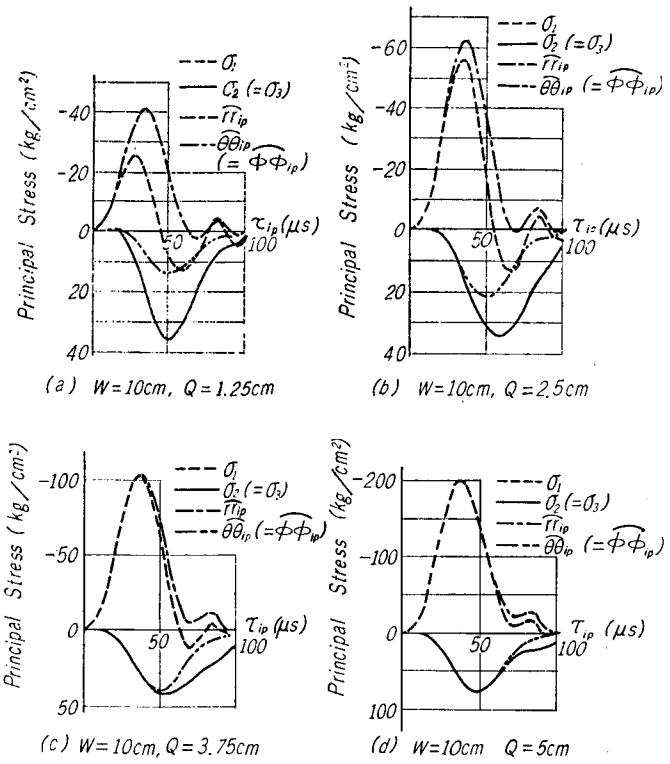

Fig. 12. Behaviour of the principal stresses in the direction of the burden.

indicates the one of which direction coincides with that of the burden and σ_2 and σ_3 indicate the ones of which directions are θ and ϕ directions, and also Q denotes the distance from the free face. Besides σ_1, σ_2 and σ_3, the stresses $(\widehat{rr}_{ip}, \widehat{\theta\theta}_{ip}, \widehat{\phi\phi}_{ip})$ which are expected to be induced at the respective point in the case where no free face exists, namely, the stresses caused only by IP are also shown in Fig. 12. Some examples of the behaviour of the principal stresses on the planes of $Q=2.5$ cm and $Q=5.0$ cm are shown in Fig. 13 [(a), (b), (c) and (d)]. The upper ones of respective figures in Fig. 13 show the change in the magnitudes of these principal stresses with time and the lower ones show the change

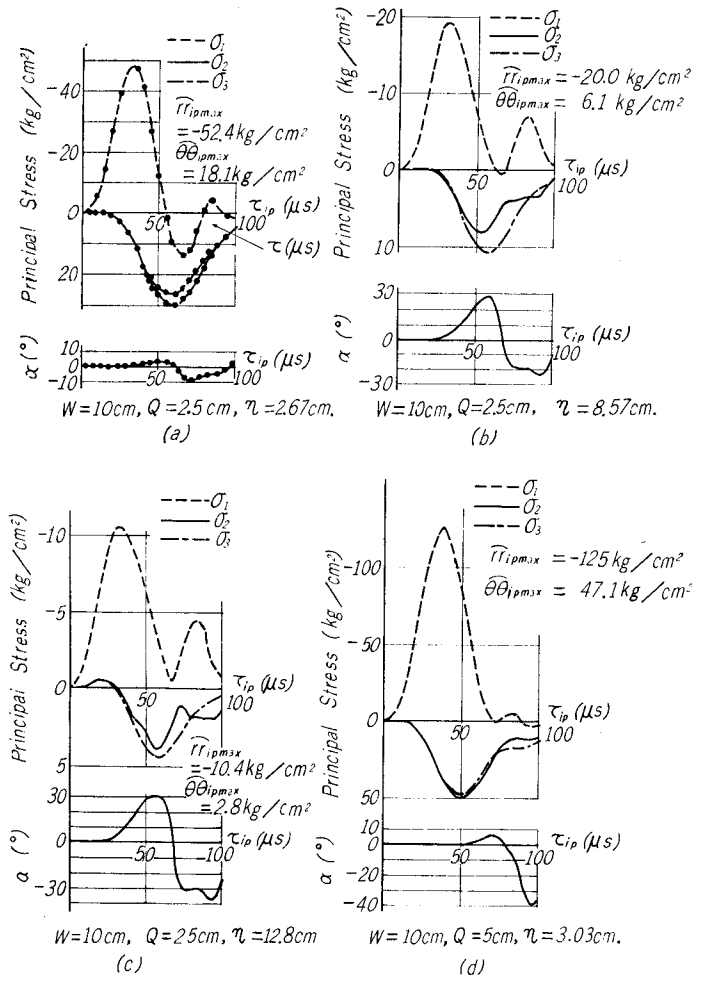

Fig. 13. Behaviour of the principal stresses near the free face.

in the direction of σ_1 with time, where α indicates $\angle$OAH as shown in Fig. 14 and its sign is prescribed as that in the case where the point H exists in the positive side of Z axis the sign is positive and inversely the sign is negative in the case where the point H exists in the negative side.

It is understood from Fig. 13 that the principal stresses σ_1, σ_2, σ_3 are composed of $\widehat{rr}_{ip}$, $\widehat{\theta\theta}_{ip}$, and $\widehat{\phi\phi}_{ip}$ respectively till the

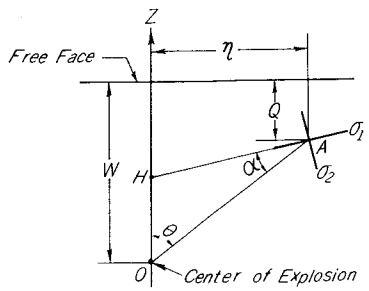

Fig. 14. Explanation of α.

reflected waves get at the respective point, but after arrival of those reflected waves the principal stresses differ from the stresses due to IP alone and the maximum compressive stress in σ_1 becomes smaller than that in $\widehat{rr}_{ip}$ and the maximum tensile stresses in σ_2 and σ_3 become larger than those in $\widehat{\theta\theta}_{ip}$ and $\widehat{\phi\phi}_{ip}$ near the free face. The ratios of the maximum compressive and tensile stresses induced within rock to those in the stresses due to IP alone are summarized in Table 3. It is understood from Table 3 that the ratios $\sigma_{2\max}/\widehat{\theta\theta}_{ip\max}$ and $\sigma_{3\max}/\widehat{\phi\phi}_{ip\max}$ increase with the approach of the free face, while the ratio

Table 3. Change in the maximum values of principal stresses due to the existence of free face.

Q (cm)	η (cm)	$\frac{\sigma_{1\max}}{\widehat{rr}_{ip\max}}$	$\frac{\sigma_{2\max}}{\widehat{\theta\theta}_{ip\max}}$	$\frac{\sigma_{3\max}}{\widehat{\phi\phi}_{ip\max}}$
1.25	0	0.61	2.64	2.64
2.5	0	0.91	1.58	1.58
	2.67	0.93	1.44	1.62
	5.36	0.95	1.29	1.62
	8.57	0.97	1.32	1.71
	12.8	1.00	1.36	1.57
3.75	0	0.99	1.13	1.13
5.0	0	1.00	1.00	1.00
	3.30	1.00	1.04	1.01
	6.06	1.00	1.21	1.03
	9.60	1.00	1.36	1.08

$\sigma_{1\max}/\widehat{rr}_{ip\max}$ decreases inversely, and at the points where the distance from the shot point is less than about 5 cm ($W/2$), the maximum value of each principal stress is influenced mainly by the stress imparted by IP. Therefore, it is found by this investigation that the maximum values of the tensile stresses induced near the free face are increased due to the existence of the free face. The relations between the maximum values in σ_1, σ_2 and σ_3 in the direction of the burden and the distance from the free face are shown in Fig. 15. As shown in Fig. 15, the maximum value of the tensile stress in $\sigma_2(=\sigma_3)$ is almost unchangeable within the range $Q<3.5$ cm and is larger than that in σ_1. The tensile stress component in σ_1 which shows its maximum value near $Q=2$ cm is caused mainly by the reflected tensile stress wave (RP) and this component is generally called as the tensile stress caused by the Hopkinson effect. The relations between the maximum values in σ_1, σ_2 and σ_3 on the plane of $Q=2.5$ cm and the distance from the burden are shown in Fig. 16. As shown in Fig. 16, the tensile stress in σ_1

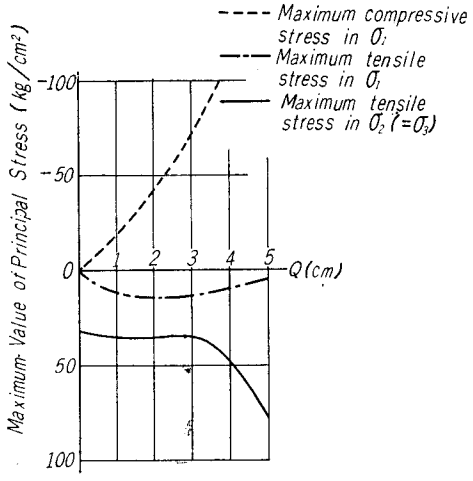

Fig. 15. Relations between the maximum values of the principal stresses in the direction of the burden and the distance from the free face.

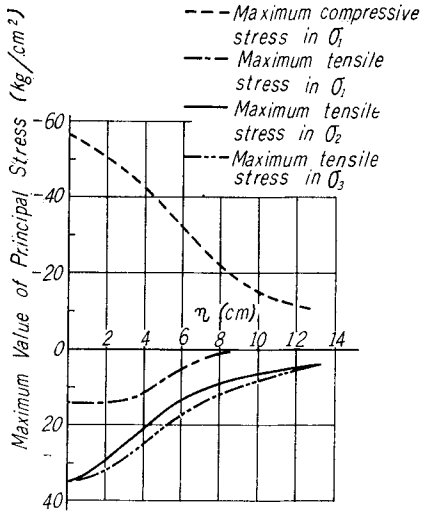

Fig. 16. Relations between the maximum values of the principal stresses on the plane of $Q=2.5$ cm and the distance from the burden.

appears only near the burden and the maximum tensile stress in σ_3 is always larger than that in σ_2 on the plane of $Q=2.5$ cm, and this relation agrees well in its tendency with that obtained by the analysis of the stresses on the free face.

Next, let us consider about the directions of σ_1 and σ_2. As shown in the lower figures in Fig. 13, the directions of σ_1 and σ_2 coincide with those of r and θ till the reflected waves get at the respective point, resulting $\alpha=0$, but after arrival of the reflected waves, the direction of σ_1 and σ_2 change with time, and

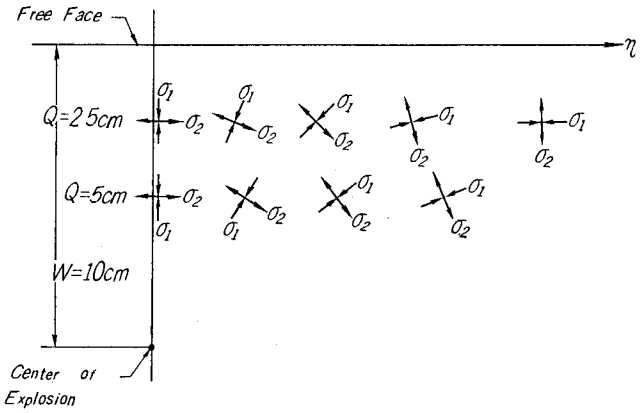

Fig. 17. Directions of σ_1 and σ_2 when the tensile stress in σ_2 attains its maximum value.

generally the sign of α starts as positive and then it changes to negative, namely, the direction of σ_1 inclines at first from the r direction towards the direction parallel to the free face and then towards the direction perpendicular to the free face. The directions of σ_1 and σ_2 when the tensile stress in σ_2 attains its maximum value are shown in Fig. 17. Fig. 17 shows that the direction of the maximum tensile stress near the free face in the $r\theta$ plane inclines gradually from the θ direction towards the direction perpendicular to the free face. It is interesting that the directions of the maximum tensile stress in the $r\theta$ plane shown in Fig. 17 are similar in its tendency to those obtained by Dr. T. Murata and Mr. K. Tanaka who have analyzed the stress distribution near the free face statically[4].

5. Appearance of Breakage Presumed from the Results of this Investigation

As the brittle rocklike material is more fragile for the tensile stress than for the compressive one, the direction of cracks may be considered to extend perpendicular to the direction of the tensile stress. Therefore, it can be understood from Fig. 17 that in case of blasting with one free face, the direction of the cracks in the $r\theta$ plane will be radial near the explosion point, but with the approach of the free face it will be curved towards the direction paralell to the free face and this tendency is more intensified with the increase of the distance from the burden. Therefore, after blasting with one free face it may be expected to produce a crater of which shape is like a lily flower. Furthermore, it is understood that as the maximum tensile stress in σ_3 is always greater than that in σ_2 at the points on and near the free face, so on the plane parallel to the free face, the radial cracks are more excellent than the concentric ones. Moreover, the cracks caused by the Hopkinson effect may be produced almost parallel to the free face, but as shown in Fig. 16, they may be limited only near the burden.

To make sure whether the appearance of the breakage presumed from this investigation is reasonable or not, some small scale crater tests were performed within the same rock mass using a detonator of No. 1 strength. An example of the profile of the crater produced is shown in Fig. 18, and a photograph of the break down rock observed from the shot side is shown in Fig. 19. By referring to these figures and to the results of the practical observations using a high speed camera[5], it may be recognized that the feature of breakage presumed by this investigation agrees fairly well with that observed in practical crater tests.

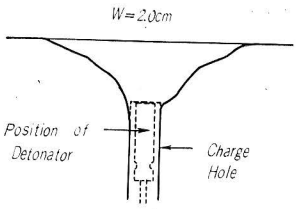

Fig. 18. Profile of crater produced.

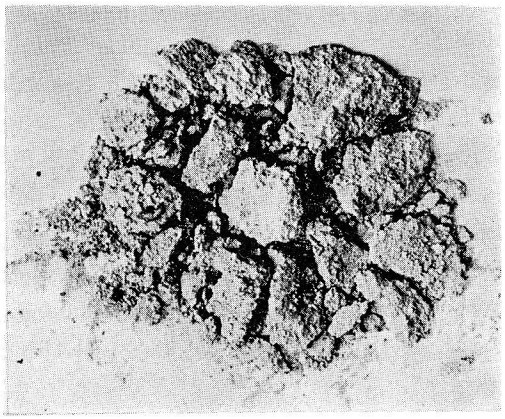

Fig. 19. Photograph of the break down rock.

Acknowledgments

The authors feel greatly indebted for the financial support received from the Ministry of Education and the Hattori Hokokai to which we also wish to express our sincere gratitude.

References

1) I. Ito and K. Sassa : This Memoirs, **23,** 70 (1961)
2) I. Ito and K. Sassa : Bulletin of Min. and Metall. Inst., Japan. (in press) (1964)
3) Ibid.
4) T. Murata and K. Tanaka : Jour. Industrial Explosive Soc., Japan. **16,** 32 (1955)
5) I. Ito, Y. Wakazono and Y. Fujinaka : Suiyōkwai-Shi (Trans. Min. and Metall. Alumni Assoc. Kyoto Univ.) **13,** 369 (1958)